Reprocessing the Blackfoot 3C-3D seismic data

Han-xing Lu and Gary F. Margrave

ABSTRACT

In November 1995, a 3C-3D survey was conducted over the Blackfoot field located near Strathmore, Alberta, Canada (T23 R23 W5M). The seismic processing was performed by Pulsonic Geophysical and Sensor Geophysical in 1996. Pulsonic processed the entire dataset whereas Sensor processed only the Glauconitic patch. The seismic survey is shown in Figure 1.

The results are quite similar on major events, but the Glauconitic results have higher signal band. Reprocessing Blackfoot 3C-3D attempted to achieve a high signal band for all the data set and to yield CDP gathers for AVO analysis and several offset-limited migrated 3D volumes for P-P and P-SV joint analysis.

Only the results of reprocessing the Glauconitic patch are presented here. The initial results for the vertical component were obtained by a conventional P-wave processing procedure. The results for the radial component include migrated, ACP (asymptotic conversion point binning) stacked section, migrated converted-wave DMO stacked section and migrated converted-wave depth-variant stacked section.

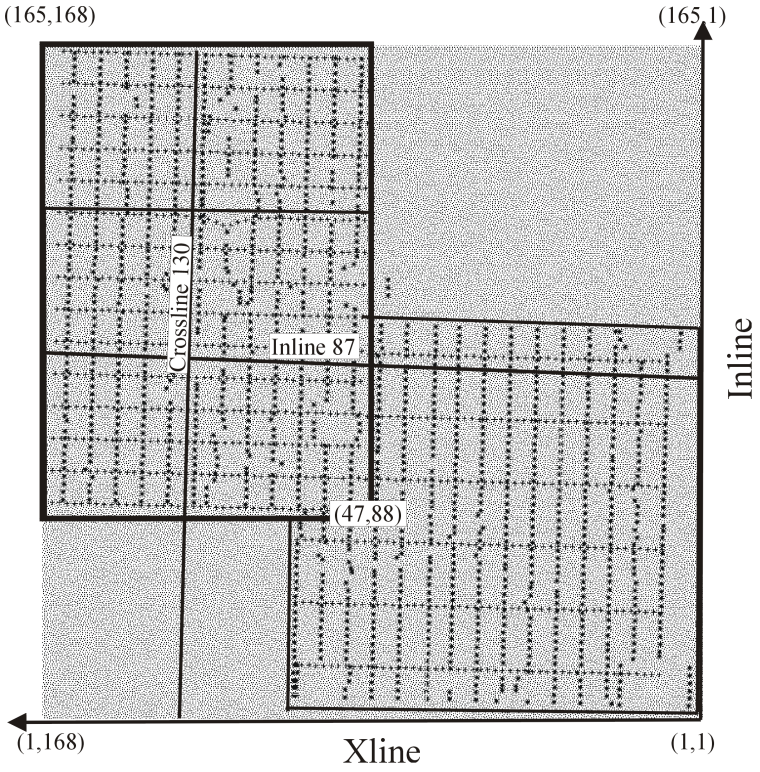

Figure 1. The seismic survey: Glauconitic patch is shown in the thick square; Beaverhill Lake patch is shown in a polygon.

Contents

INTRODUCTION

The Blackfoot 3C-3D survey covered an area of 16.8 square kilometers and consisted of two distinct patches. These two patches have the same source pattern: 60m source interval and 210m source-line spacing. The high fold patch, targeting Glauconitic channel sands of lower Mannville, has 60m group interval and 255m receiver-line spacing. The long offset patch targeting deeper Swan Hills reef-prone carbonates has 60m receiver group interval and 495m receiver-line spacing. Figure 2 shows the CDP fold map (offset 0-2900m) for the vertical component (maximal fold is 121) and ACP (Asymptotic approximation binning, Vp/Vs=2.2) fold map (offset 0-3240m) for the radial component (maximal fold is 120). The P-SV fold map shows larger fold toward the edge of the survey area than the P-P fold map. The geology and exploration targets are described more fully in Margrave et al. (1998).

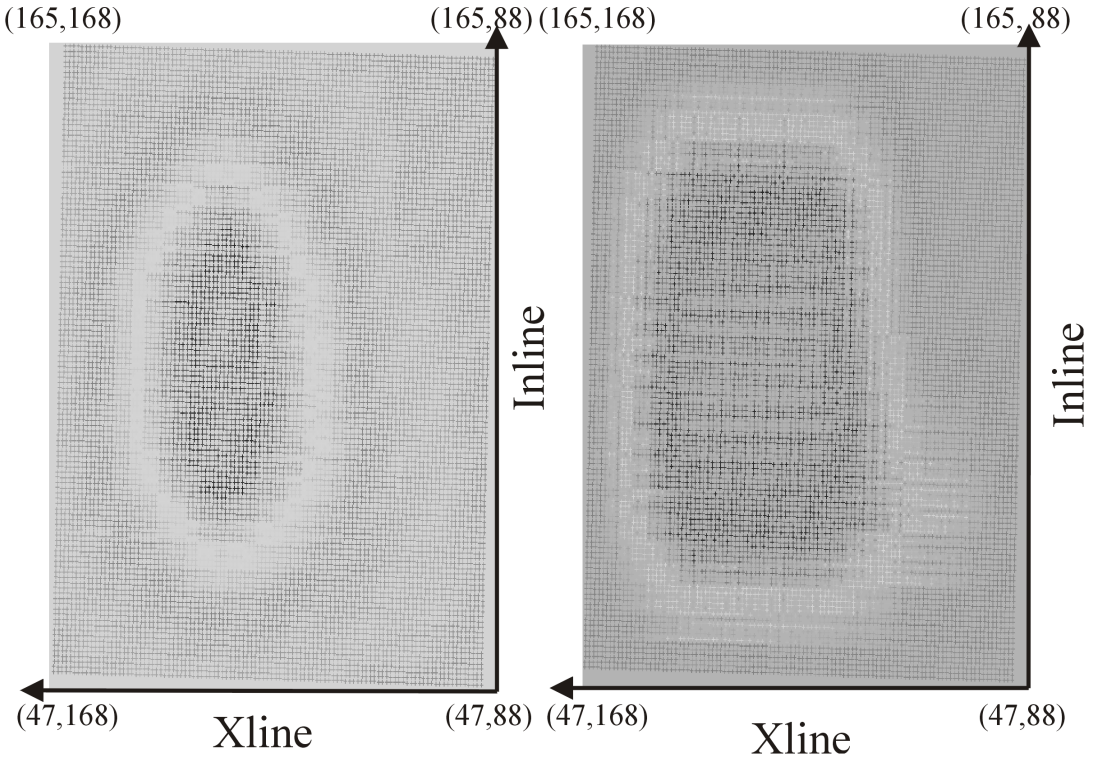

Figure 2. The fold map for vertical (offset 0-2900m) is shown on the left; the fold map for radial (0-3240m) after ACP binning is shown on the right.

DATA

The shot gathers were separated into vertical, north (H2) and east (H1) components before processing the data. Fig.3 (a), (b), (c) show the separated three components, (d), (e), show the radial and transverse components after rotation.

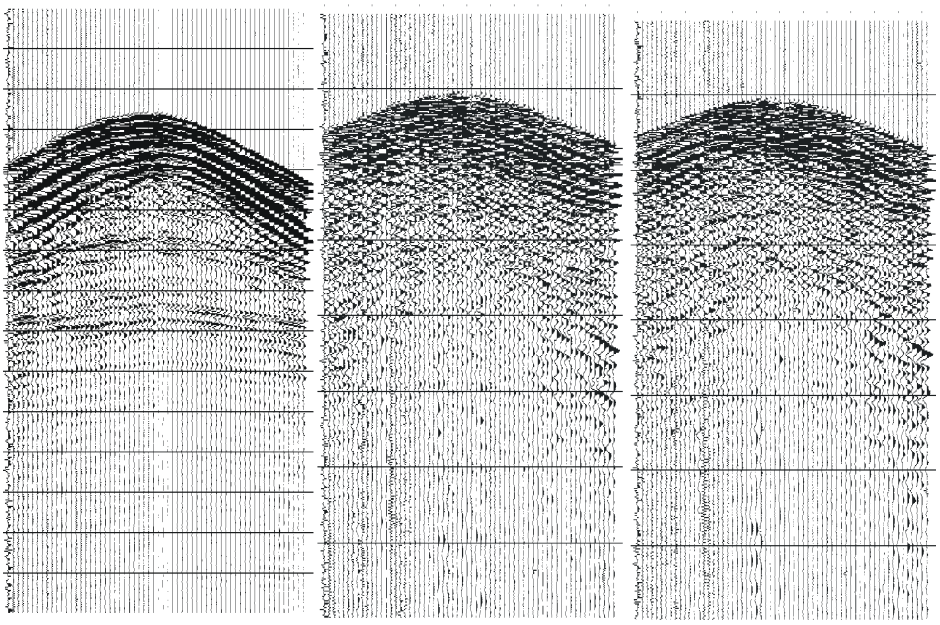

(a) (b) (c)

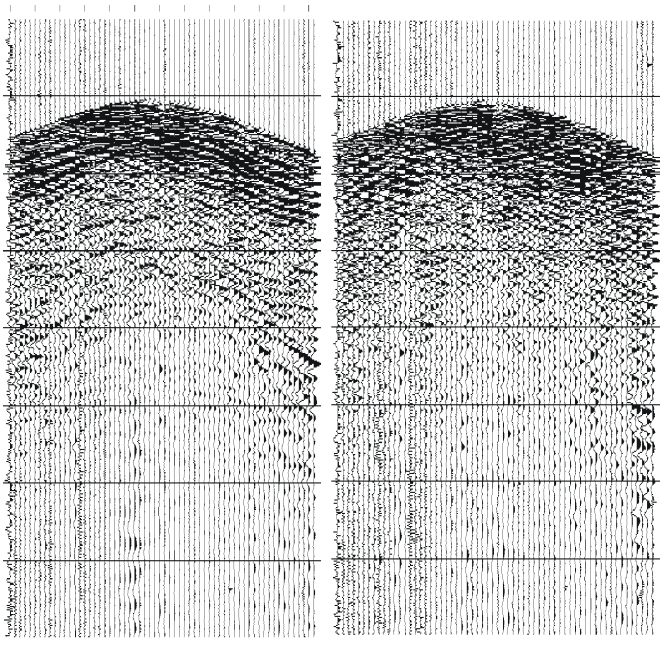

(d) (e)

Figure 3 (a), (b), (c) Vertical, horizontal-east and horizontal-north components, (d), (e) radial and transverse components for a portion of shot 18.

Contents

After component separation, geometrical rotation was applied to north and east components to generate radial components towards the source and transverse components orthogonal to the radial components. After rotation, the vertical component data shows quite high signal/noise ratio and the data of radial component shows reasonable signal/noise ratio, while the transverse component shows little energy (see Figure 3d, 3e).

PROCESSING FLOW

The seismic processing software package 'ProMAX" was used for data processing. The raw records were input from de-multiplexed SEG-D tape. The 2070 channel shot records (Glauconitic patch) were separated into three individual datasets of 690 records of vertical, radial and transverse component (Figure 3a, 3b and 3c).

Testing on the data included filter and deconvolution tests on the vertical and radial raw records to determine the output spectrum for deconvolution and display filter for quality control.

Deconvolution tests were performed including spiking decon and surface consistent decon (spiking operator) with different operator lengths and pre-whitening parameters. After testing, the surface consistent decon was chosen. Source, receiver, offset and CDP were chosen for spectral decomposition, but only the source and receiver components were applied.

Processing with or without refraction static corrections and with or without spectral whitening were also tested. After evaluation, a routine processing flow was chosen for vertical component reprocessing. The processing flow for vertical component is as follows:

Table 1. Processing sequence for the vertical component data.

SEG-D FORMATTED DE-MULTIPLEX INPUT
3D GEOMETRY ASSIGNMEMT
TRACE EDIT
TRUE AMPLITUDE RECOVERY
SURFACE CONSISTENT DECONVOLUTION
TIME VARIANT SPECTRAL WHITENING
ELEVATION AND REFRACTION STATIC CORRECTIONS
VELOCITY ANALYSIS
RESIDUAL SURFACE CONSISTENT STATICS
NORMAL MOVEOUT
TRIM STATICS
FRONT END MUTING
CDP STACK
TIME VARIANT SPECTRAL WHITENING
TRACE EQUALIZATION
F-XY DECONVOLUTION
3D PHASE-SHIFT MIGRATION
FOR TRACE DISPLAY:
TRACE EQUALIZATION
BANDPASS FILTER
TIME VARIANT SCALING

Velocity analysis was performed using a grid of 600m by 600m for the vertical component. Phase-shift 3D migration (single pass) was used for migration and 100% stacking velocities were used for vertical component migration.

The reprocessing flow for Radial component is as follows:

Table 2. Processing sequence for the radial component data.

SEG-D FORMATTED DE-MULTIPLEX INPUT
COMPONENTS SEPARATION
3D GEOMETRY ASSIGNMENT
TRACE EDIT
ASYMPTOTIC BINNING
SURFACE CONSISTENT DECONVOLUTION
TIME VARIANT SPECTRAL WHITENING
ELEVATION STATICS
APPLY FINAL REFRACTION AND RESIDUAL STATICS FROM P-P
CONSTRUCT INITIAL P-SV VELOCITY FROM FINAL P-P VEL.
VELOCITY ANALYSIS
RECEIVER RESIDUAL STATICS (HAND STATICS)
VELOCITY ANALYSIS
CONVENTIONAL RESIDUAL STATICS
VELOCITY ANALYSIS
NORMAL MOVEOUT
ACP TRIM STATICS
FRONT END MUTING
ACP STACK (DEPTH-VARIANT STACK AND DMO STACK)
TIME VARIANT SPECTRAL WHITENING
TRACE EQUALIZATION
F-XY DECONVOLUTION
3D PHASE-SHIFT MIGRATION
FOR TRACE DISPLAY:
TRACE EQUALIZATION
BANDPASS FILTER
TIME VARIANT SCALING

The conversion point binning was performed by the approximate asymptotic binning method (Harrison, 1992), using an average Vp/Vs. The same Vp/Vs was used to construct the initial P-SV stacking velocity. Velocity analysis was performed using a grid of 600m by 300m.

Residual receiver static corrections as large as 150 ms were found in reprocessing the radial data. Because of this large static correction, the traditional statics programs (usually for both source and receivers) do not perform well. In this case, applying the final P-P statics to the source is acceptable for source statics for the radial component (Harrison, 1992).

To solve the statics problem, the common receiver stack method was used. The common-receiver stacks can give a clear indication of residual receiver statics. But this method is restricted to the areas which have small lateral changes in reflector time (e.g. no significant structure). Figure 4 shows a portion of a receiver stacked section before and after applying receiver statics. We also had a residual statics

problem between the Glauconitic patch and the Beaverhill Lake patch, This remains unsolved, so only the results of the Glauconitic patch are presented at this time.

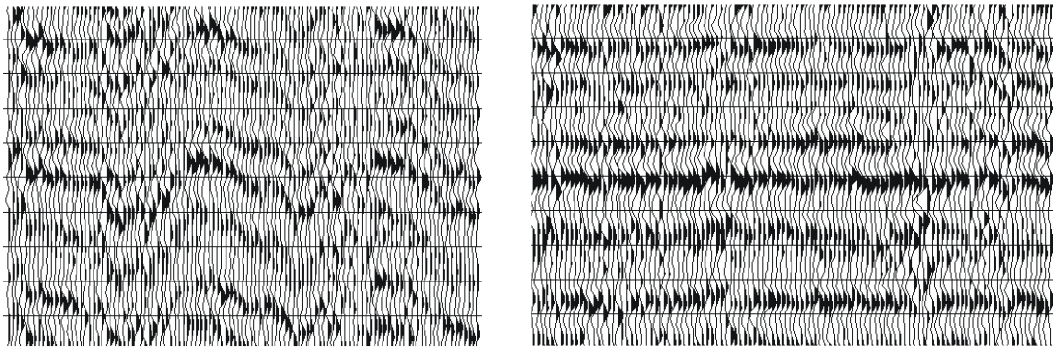

(a) (b)

Figure 4 A portion of receiver stacked section before and after receiver statics applied.

After removing the large receiver statics, a conventional surface-consistent method can be used to remove any remaining source and receiver statics.

After ACP stacking, Vp/Vs for different time windows was extracted via visual comparison of the vertical and radial sections. A converted-wave depth-variant stack was performed to improve conversion point binning (Cary et al., 1993). In order to attenuate noise and improve binning for dipping events, converted-wave 3D DMO and 3D DMO stack were tested. Offset binning size was 180 m, three times the shot interval, because of the flat structure. In this case, because the events are quite flat, there shouldn't be a big difference between converted-wave depth-variant stack and converted-wave 3D DMO stack. Phase-shift migrations were performed on all the stacked sections, 97% stacking velocities were used for migration.

The Glauconitic channel interval seen in Figure 5 are on migrated stacked sections.

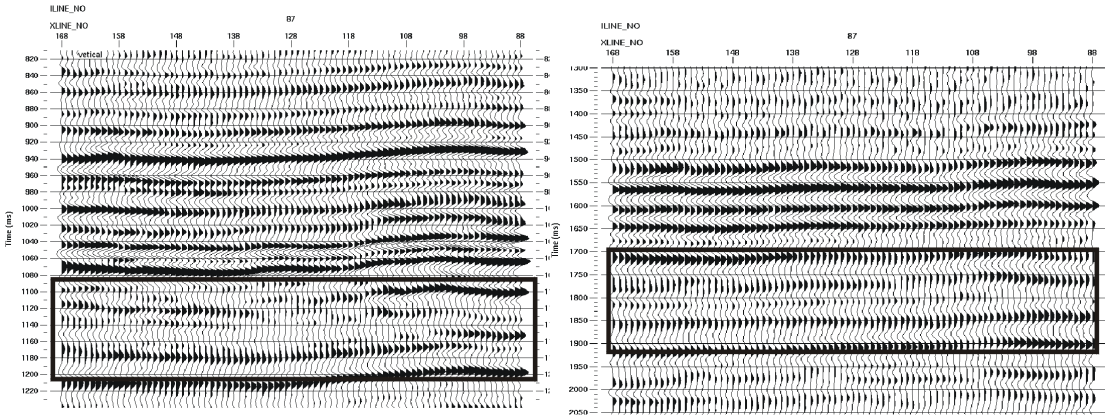

(a) (b)

Figure 5 Channel cuts are shown on vertical migrated stacked section at around 1080ms (a); also are shown on radial migrated section at about 1750 ms (b).

Contents

Implicit finite difference time (FD) migration and phase-shift (PS) migration were tested on the ACP stacked data. In general, FD migration has less edge effect and less migration noise than PS, and can handle lateral variation of velocities; however, FD migration takes more compute time. The results for a time window encompassing the channel are very similar, so the phase-shift migration method was chosen.

For comparison, the migrated ACP stacked section, the converted-wave DMO 3D stacked section and converted-wave depth-variant stacked section are shown in time window for channel (Figure 6).

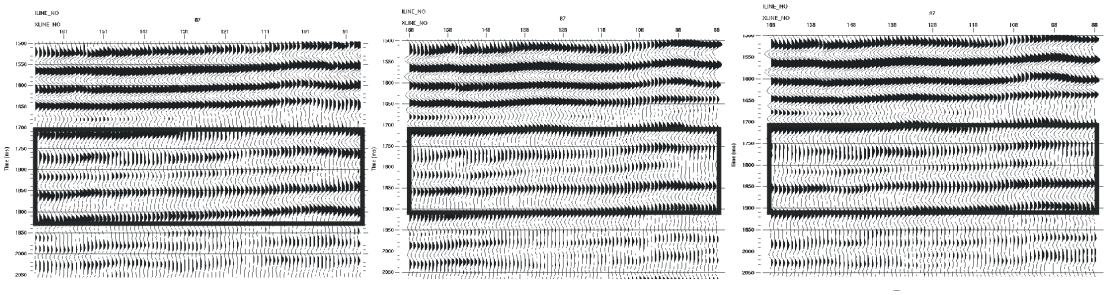

(a) (b) (c)

Figure 6 Glauconitic channel cuts are shown in squares: (a) The channel cuts are shown on migrated ACP stacked section; (b) on migrated depth-variant stacked section and (c) on migrated 3D DMO stacked section.

From Figure 6 we can see the amplitude differences between ACP stacked data and the others, but the results of depth variant and DMO stacked sections are similar.

The migrated stacked sections for P-P (offset 0-2900m) and P-SV (offset 0-3240m) are shown in Figure 7.

The average spectra of migrated stacked sections for vertical and radial components are shown in Figure 8. The final signal bandwidth was estimated for P-P and P-SV data.

DATA PRODUCTION

The other motivation for reprocessing Blackfoot 3C-3D is to produce CDP and ACP gathers for future AVO analysis, and to produce migrated offset-limited stacked sections for P and P-SV joint inversion to get better rock property estimates (Stewart, 1990, Margrave et al., 1998).

These data (Glauconitic patch) are now available:

1. Vertical-component CDP gathers after true amplitude recovery, surface-consistent decon and TV whitening (or without TV whitening), with statics applied.

2. Radial-component ACP gathers after true amplitude recovery, surface-consistent decon and TV whitening (or without TV whitening), with statics applied.

3. Several offset-limited stacked sections were migrated for vertical and radial components.

4. Datasets 1 and 2 after NMO correction.

CONCLUSION

Standard seismic processing flows produced good results for P-P data. 2-C rotation results suggest that the birefringence in this case was negligible. However, we should stack up the transverse component to see (using the exact processing flow for radial component). Three binning methods (asymptotic approximation, depth-variant, 3D DMO) showed that ACP binning presented good initial results. Converted-wave 3D DMO binning should give the most accurate results, but in this case, because of flat structure, the converted-wave depth-variant method and 3D DMO method gave similar results. The initial velocity function for P-P was taken from 2-D processing results from Blackfoot field.

The results of reprocessing the Glauconitic patch are similar on the major events compared with the results of Pulsonic and Sensor (see CREWES Research Report 1996, vol. 8). Our results are a little noisier, especially in the low ACP fold area for the radial component, in order to preserve the relative amplitudes, no further visual enhancement steps (such as trace mixing, spatial filtering) were applied.

FUTURE WORK

For better CDP fold for the channel, the full data set (Glauconitic and Beaverhill Lake patches) should be processed together. Post-stack depth migration will be tested on this 3C-3D dataset.

We still have a statics problem between the two patches for the radial component, only the results of Glauconitic patch is presented here at this time.

The inhomogeneity and anisotropy of media have more effect on the converted wave data than pure-mode data (Thomsen, 1998). In this reprocessing the Vp/Vs (ratio of average velocity) was held constant for asymptotic binning. Depth variant and DMO binning were performed to attempt to get accurate conversion point using variable Vp/Vs within different time windows. In a laterally inhomogeneous medium, physical properties must be considered more carefully. In order to get a more accurate conversion point, especially for precise depth image, an effective velocity ratio, $\gamma_{eff,}$ probably should be applied.

ACKNOWLEDGMENT

We would like to thank the sponsors of the CREWES project for their financial support of this work. We also thank our colleagues in CREWES for their work involved in this project.

REFERENCES

Margrave Gary. F., Lawton, D. C., and Stewart, R. R., 1998, Interpreting channel sands with 3C-3D seismic data: April, The leading Edge.

Cary, P., Pye, G., and Harrison, M., 1993, New methods in processing converted-wave data: paper presented at the 1993 CSEG national convention.

Harrison, M., P., 1992, Processing of P-SV surface seismic data: anisotropy analysis, dip moveout, and migration: Ph.D. dissertation, University of Calgary.

Thomsen, L., 1998, Converted-wave reflection seismology over inhomogeneous, anisotropic media: Accepted for publication Geophysics.

Stewart R. R., 1990, Joint P and P-SV inversion: The CREWES Project, Research Report vol. 2.

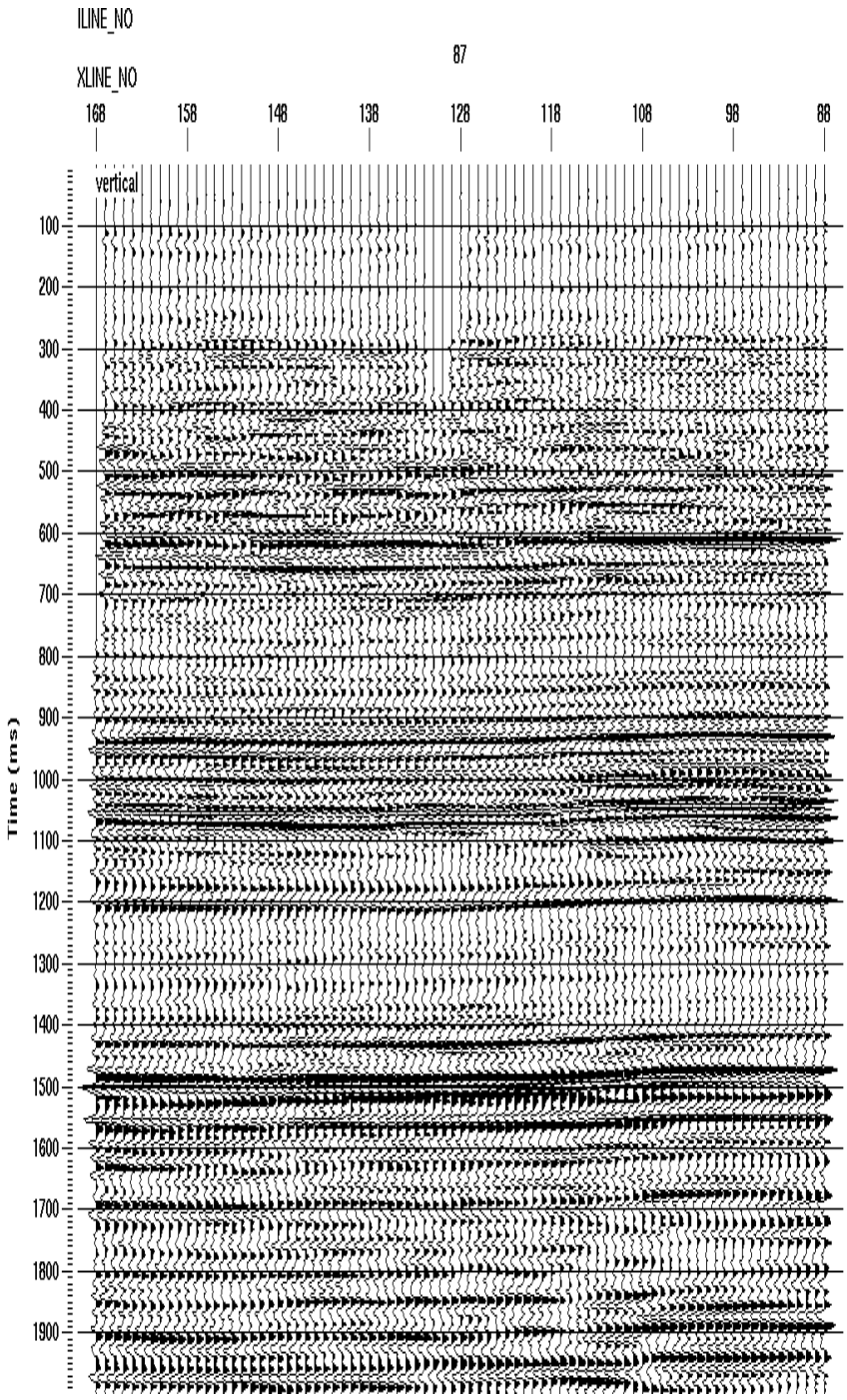

Figure 7a. Migrated P-P stacked section for inline 87.

Contents

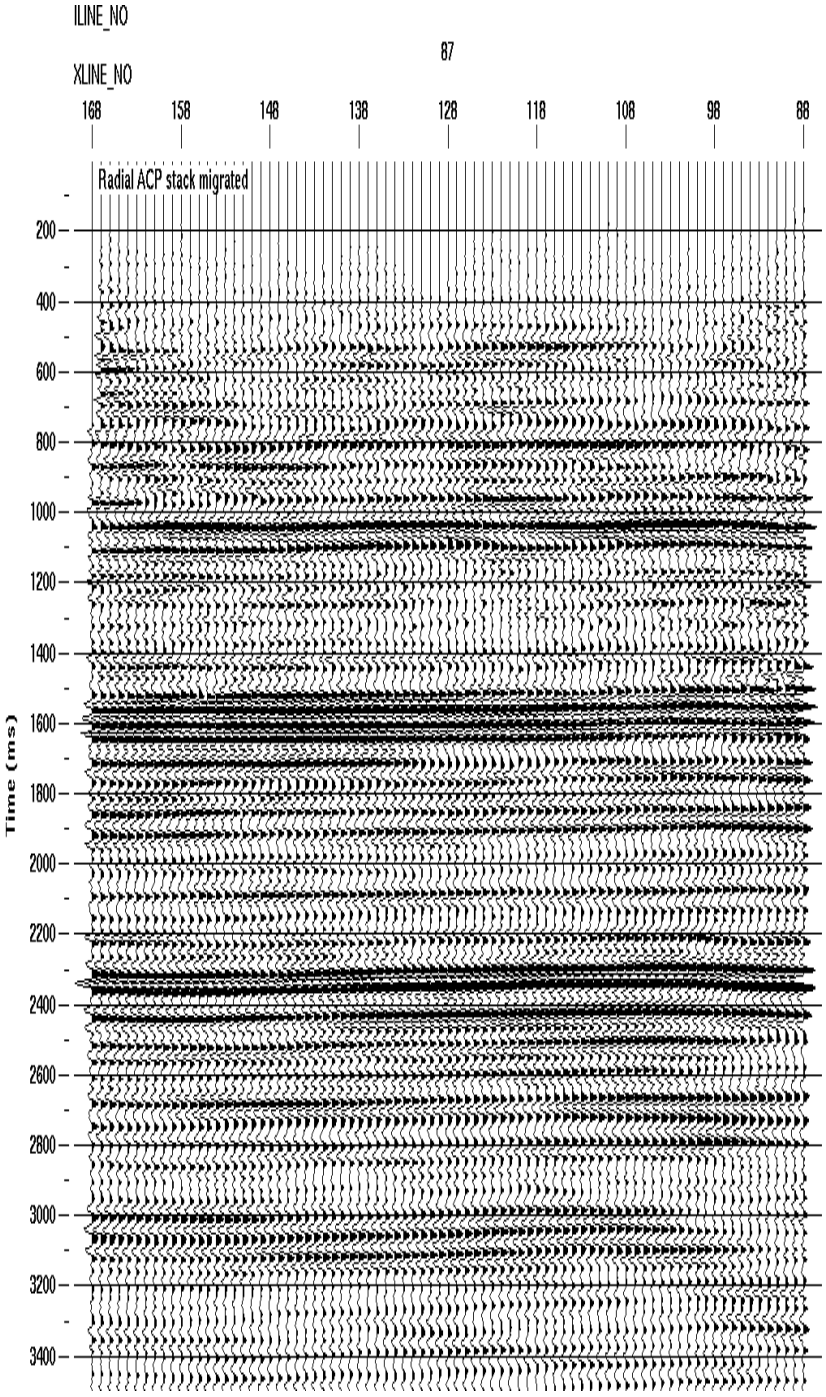

Figure 7b Migrated ACP stacked section for inline 87.

Contents

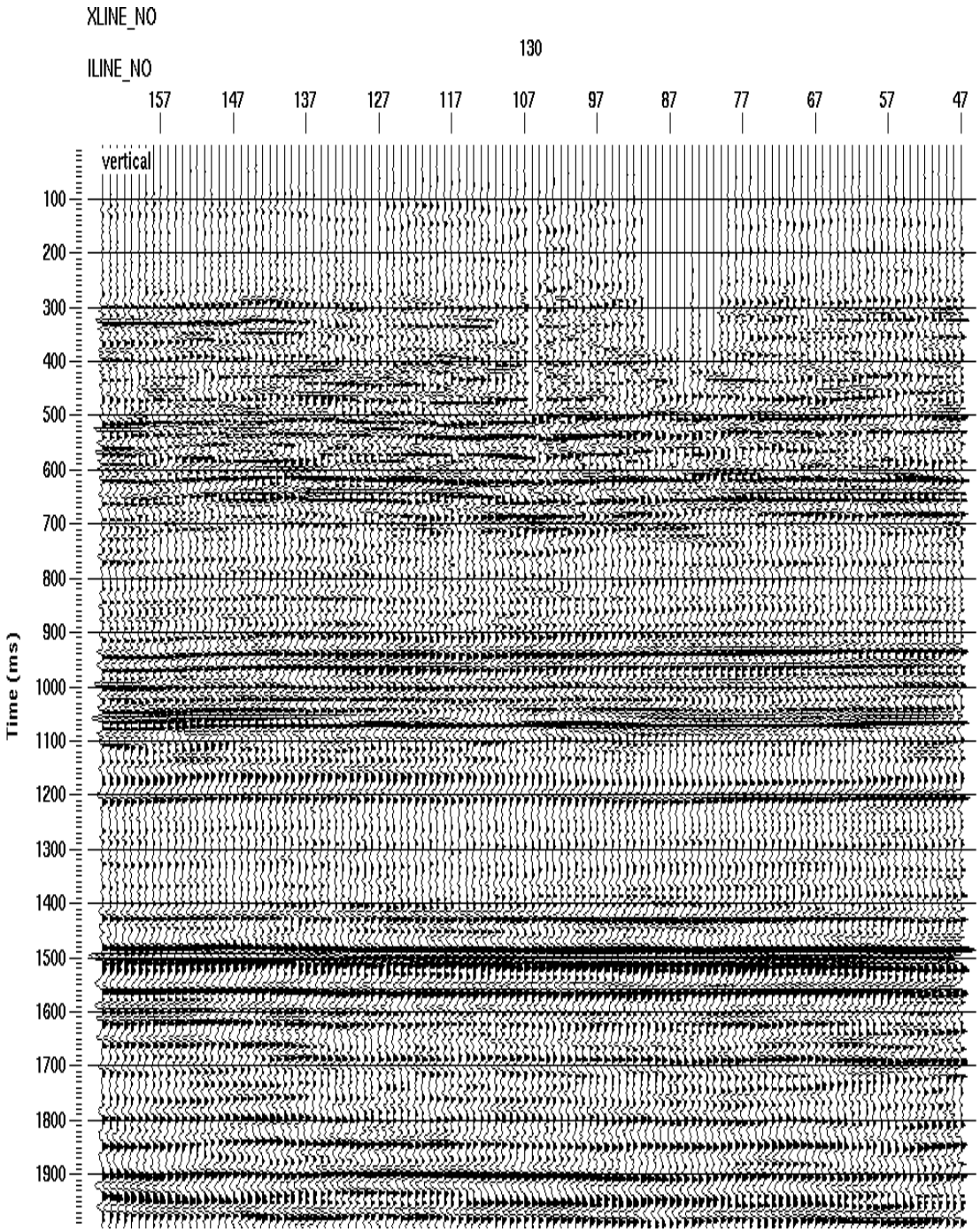

Figure 7c Migrated P-P stacked section for cross-line 130.

Contents

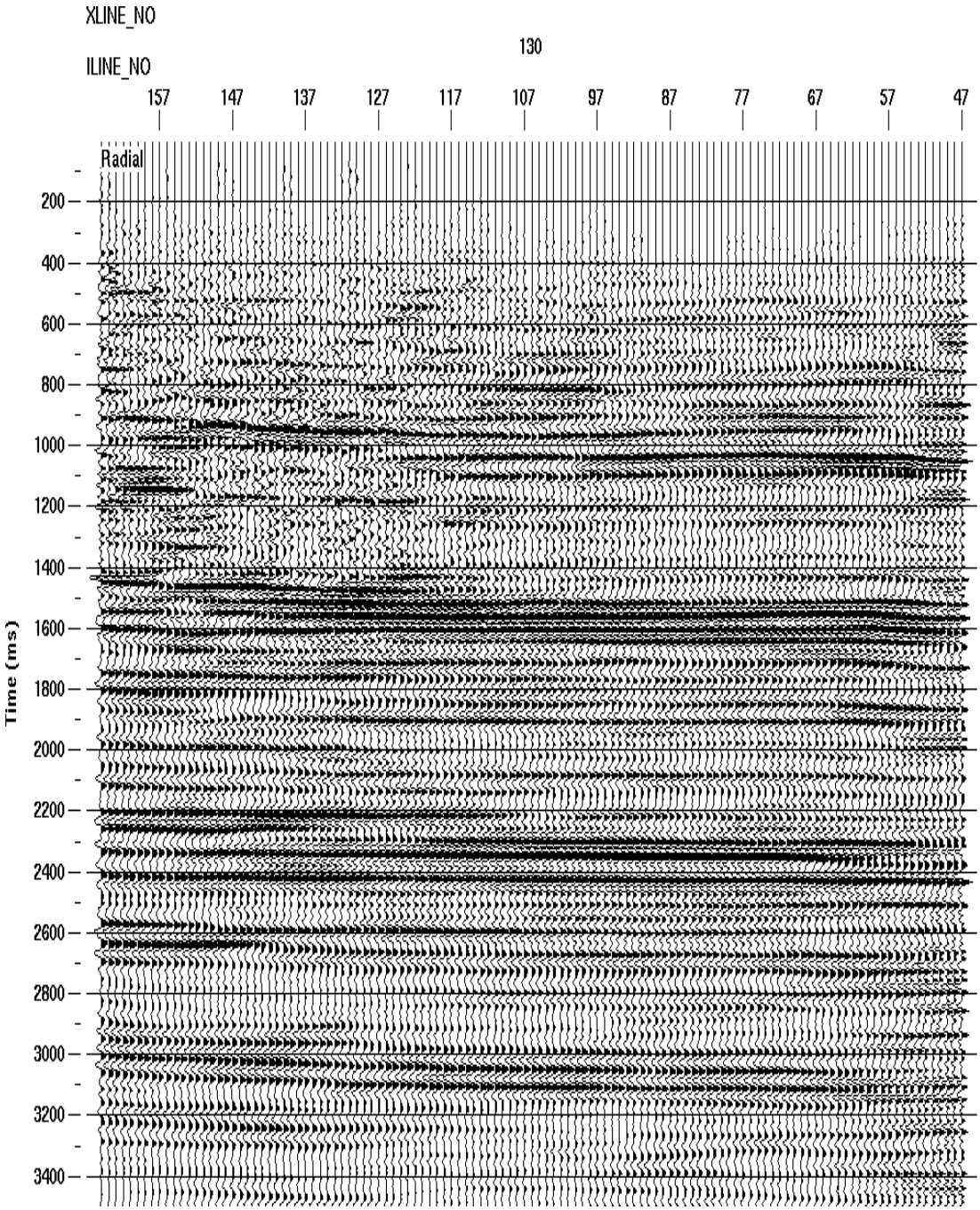

Figure 7d Migrated ACP stacked section for cross-line 130.

Contents

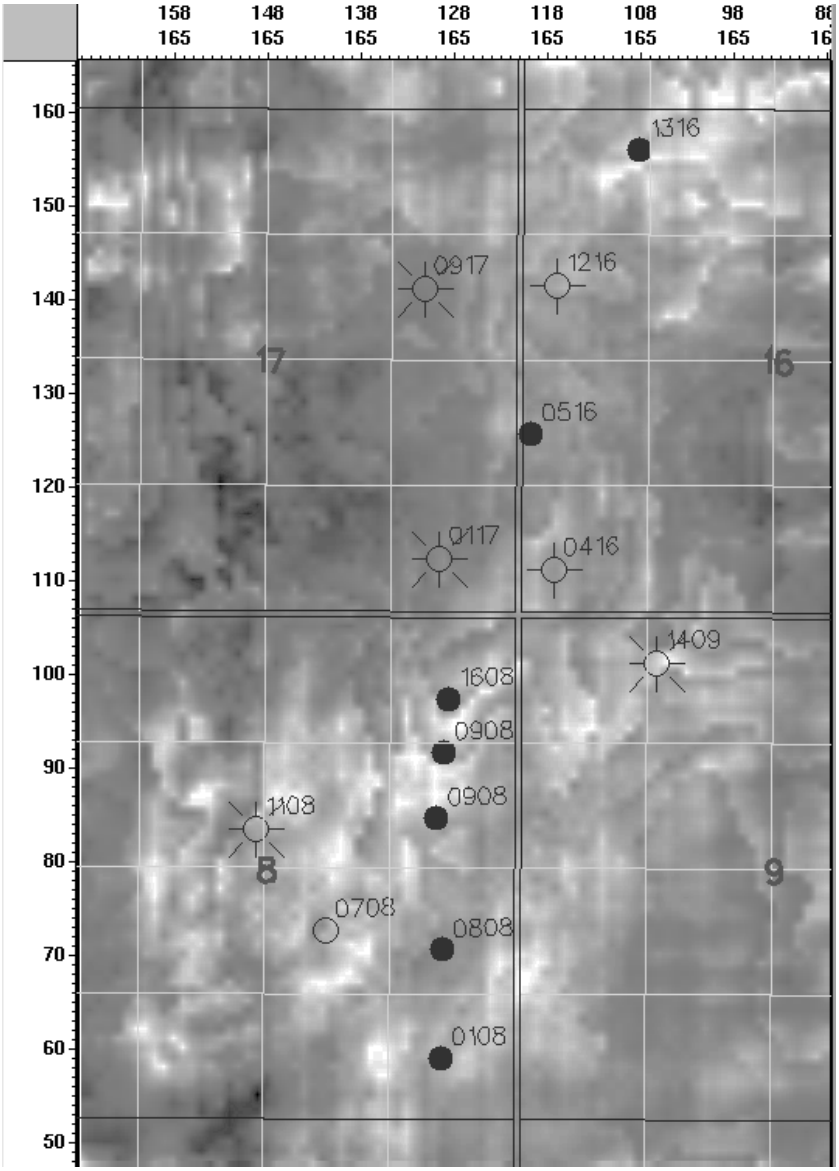

Figure 7e. Time slice at 1080ms after data were flattened on the low Mannville event for the vertical component. Solid dots are producing wells.

Contents

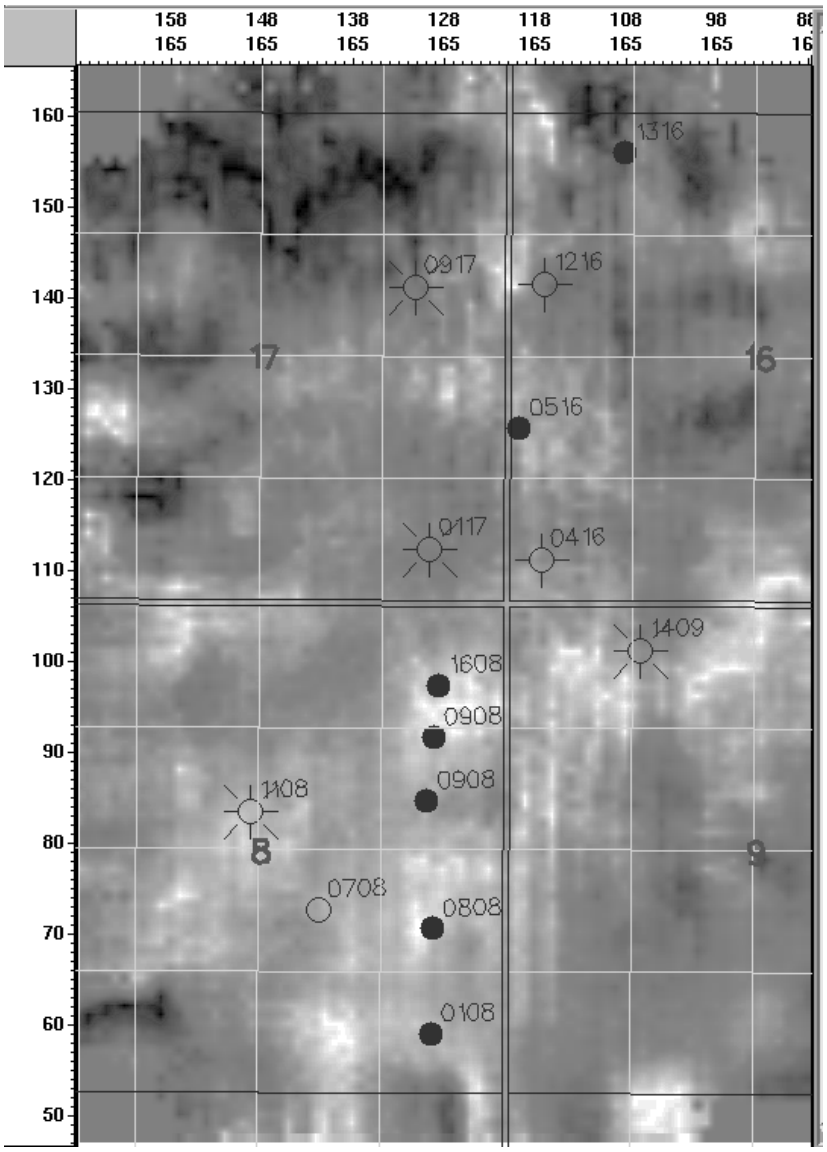

Figure 7f Time slice at 1746 ms for the radial component after data were flattened on low Mannville event, solid dots are producing oil wells.

Contents

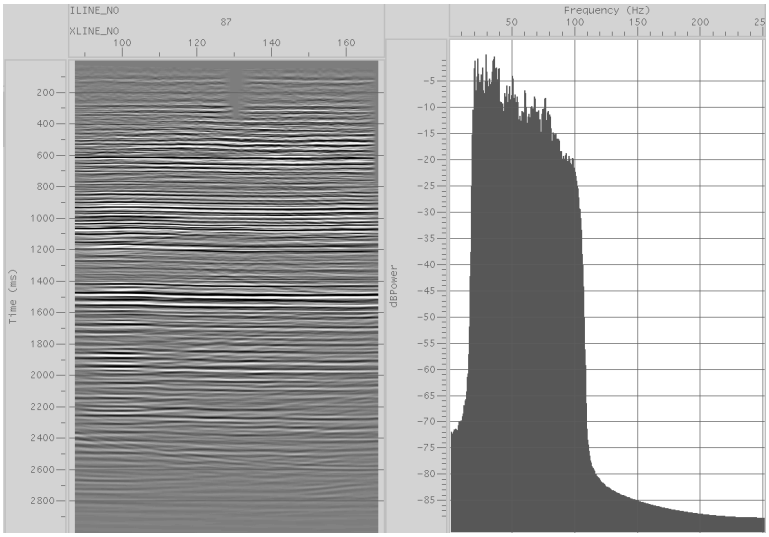

a

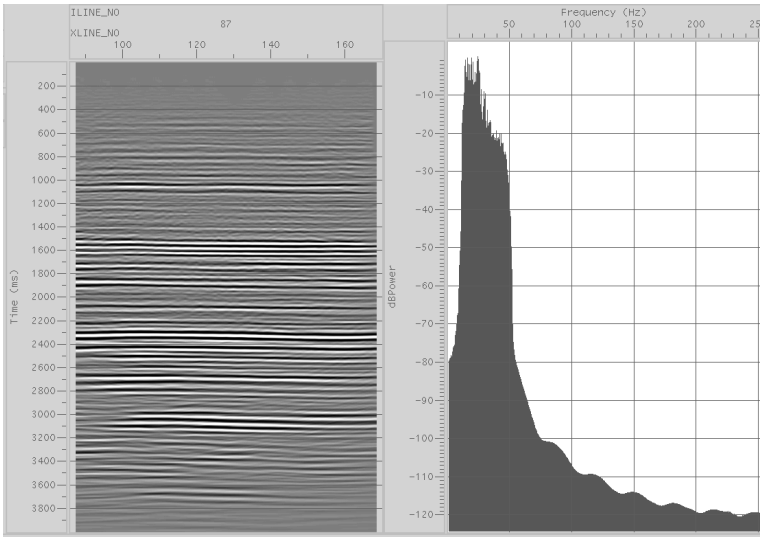

b

Figure 8 Average spectra for migrated stacked sections for the vertical (a) and the radial (b) components.

Contents